Heat Transfer Engineering, 30(9):751–761, 2009
Copyright © Taylor and Francis Group, LLC
ISSN: 0145-7632 print / 1521-0537 online
DOI: 10.1080/01457630802678573

Taylor & Francis
Taylor & Francis Group

Simultaneously Developing Flows Under Conjugated Conditions in a Mini-Channel Array: Liquid Crystal Thermography and Computational Simulations

Downloaded By: [Technische Universiteit - Eindhoven] At: 14:34 14 June 2009

MANOJ RAO and SAMEER KHANDEKAR

Department of Mechanical Engineering, Indian Institute of Technology Kanpur, Kanpur, India

This work presents experimental and computational calculations concerning thermo-hydrodynamics of simultaneously developing single-phase liquid flow in a semicircular mini-channel array subjected to conjugate thermal boundary conditions. Inherently, such developing flow conditions give higher species transfer coefficients. The understanding of transport processes in such systems is important because of its potential widespread use in many engineering systems. An array of seven parallel semicircular channels (internal diameter = 3.0 mm, hydraulic diameter = 1.83 mm, and length = 200 mm) was milled on a copper substrate (200 × 85 × 5 mm^3). The interchannel pitch was 6.0 mm. Liquid crystal thermography was employed to measure spatial steady-state distribution of wall/fluid temperatures over the array. This technique was chosen to (i) obtain spatial field information needed for analyzing developing flows and (ii) overcome the limitations posed by conventional techniques when employed on small geometries. A differential transducer measured the pressure drop across the array. The flow experimental Reynolds number varied from 300 to 3200. The working fluid employed was distilled, deionized, and degassed water. A three-dimensional (3D) computational grid, representing the physical domain of the experiment, was generated and conservation equations were solved on a commercial platform. The results of the study show that: (a) Conventional theory, which predicts thermo-hydrodynamics of internal flows, is well applicable for the channels used in this study. The experimental Poiseuille number and Nusselt number under laminar as well as turbulent flow conditions closely matched with those generated by the computation model. Experimental data suggests that transitional flows existed between Reynolds number 800 and 1500. (b) Although with some limitations, liquid crystal thermography is well suited for mini-/micro-scale applications, especially for studying developing flows. (c) Wall conduction effects cannot be neglected under certain boundary/experimental conditions (d) A realizable k–ε model was found to be more suitable for turbulent flow modeling in mini-channels.

INTRODUCTION

The need for economically viable, energy-efficient, compact heat transfer systems is increasing day by day. In this context, advances in fabrication technologies have led to a vast array of miniaturized devices in diverse engineering fields. Miniaturized electronic components, fuel cells, biomedical equipment, aerospace thermal systems, compact heat exchangers, and refrigeration systems are a few examples. Successful implementation of flows in these miniaturized devices necessitates understanding of the underlying transport processes. For the purpose of designing mini-channel flow-based devices utilizing single-phase fluid flow, the most important parameters of interest are the flow friction factor (approximately the Poiseuille number, Po) and the heat transfer coefficient (approximately the Nusselt number, Nu).

It is well known that species transport is highly augmented and enhanced during developing flows. This is a strong motivation for its application, especially in mini-/micro-scale circumstances, of course with a penalty of additional high wall

Address correspondence to Dr. Sameer Khandekar, Department of Mechanical Engineering, Indian Institute of Technology Kanpur, Grand Trunk Road, Kanpur (UP) 208016, India. E-mail: samkhan@iitk.ac.in

momentum flux leading to increased pumping power requirements. While a large body of literature, analytical as well as experimental, focuses on fully developed flows, developing flows, typically those that are simultaneously developing, have been lesser reported on a comparative scale, especially in mini/micro regimes [1–4].

In this article we focus on simultaneously developing flows in semicircular mini-channels. A semicircular geometry can be viewed as segment of a circular section or, alternatively, it is a limiting case of a circular tube with a twisted tape, when the pitch of the tape approaches infinity; only limited data are available for this geometry [1, 3]. Shah and London [1] report some work done on semicircular sections/circular segments but under fully developed conditions. Both, uniform heat flux and heat flux applied to the curved portion only (diametrical arc is insulated) have been considered. Correlations for simultaneously developing flows are not readily available, and Kandlikar et al. [4] highlight the need for generating this data for benchmarking.

In this background, we report experimental pressure drop and liquid crystal thermographic (LCT) measurements, leading to the estimation of the streamwise Nusselt number (Nu_x), over a semicircular mini-channel array (D = 3.0 mm, D_{hyd} = 1.83 mm, L = 200 mm) under simultaneously developing and conjugate thermal conditions. We compare the results with three-dimensional (3D) computational calculations performed under boundary conditions similar to those prevailing in the experiments.

LITERATURE REVIEW

From a historical perspective, Poiseuille, Darcy, Fanning, Mises, and Nikuradse,[1] among others, did the pioneering work to relate the pressure drops in pipes to various parameters like relative roughness, flow Reynolds number (Re), and transition from laminar to turbulent flow. Later, Colebrook proposed a well-known correlation in the year 1939. Moody presented Colebrook's results in a graphical format correlating f_{darcy} as a function of flow Reynolds number (laminar and turbulent regions) over a relative roughness (e/D) range of 0 to 5% in the year 1944. In laminar region, relative roughness shows very little effect on the overall pressure drop. In contrast, in turbulent region, f_{darcy} increases with Re and asymptotically reaches a constant value at higher Re; this asymptotic value increases with increasing relative roughness [1–4].

In the recent past, the focus has changed from macro-sized flow channels/pipes to mini/micro counterparts. This is a natural outcome of the quest for higher species transport rates per unit volume of the equipment. While there is no clear demarcation of mini/micro geometrical regimes, according to Kandlikar and Grande [5], a tentative scheme is as follows:

- Conventional channels $D_{hyd} > 3.0$ mm
- Mini-channels 3 mm $\geq D_{hyd} \geq 200\mu$ m
- Micro-channels 200 μm $\geq D_{hyd} \geq 10\mu$ m

Other ways of classification could be, for example, based on some relevant nondimensional numbers of interest, viz., Bond number, Knudsen number, or Confinement number. As regards the friction factor in mini/micro systems, the earliest studies were reported by Wu and Little [6], who studied silicon and glass microchannels having trapezoidal cross-section with a D_{hyd} = 55.81, 55.92, and 72.38 μm. Gases were used as test fluids (N_2, H_2, Ar); the measured values of f_{darcy} were larger (10–30%) than those predicted by the conventional theory. The authors concluded that the deviations are due to large e/D and its asymmetric distribution on the channel walls. The potential of micro-channels in high heat flux removal application was first highlighted by the pioneering work of Tuckerman and Pease [7]. The experimental investigations that followed in the next 10 years focused on single-phase thermo-hydrodynamics in these channels. A range of inconsistent and conflicting results has also been reported, mainly attributable to experimental uncertainties, sensor intrusion, ill-defined experimental boundary conditions, effect of roughness, etc.

The single-phase forced convective heat transfer characteristics of water/methanol flowing through micro-channels with rectangular cross section were experimentally investigated by Wang and Peng [8] with five different combinations, maximum and minimum channel size varying from (0.6×0.7 mm^2) to (0.2×0.7 mm^2). The results provide significant data and considerable insight into the behavior of the forced-flow convection in micro-channels.

The single-phase forced convective heat transfer micro-channel structures/plates with small rectangular channels having hydraulic diameters of 0.133–0.367 mm and distinct geometric configurations were investigated experimentally by Peng and Peterson [9]. The results indicated that the geometric configuration had a significant effect on the single-phase convective heat transfer and flow characteristics. The laminar heat transfer was found to be dependent upon the aspect ratio and the ratio of D_{hyd} to the center-to-center distance of the micro-channels. The turbulent flow resistance was usually smaller than that predicted by classical relationships. The Reynolds number corresponding to flow transition to fully developed turbulent flow became much smaller than the ordinary channel flow ($\approx$400–900). Empirical correlations were suggested for calculating both the heat transfer and pressure drop.

Experiments by Adams et al. [10] reported heat transfer results for water flowing through circular channels of diameters 0.76 and 1.09 mm. The data for Nu was found to be higher than what would be predicted by traditional correlations. Gao et al. [11] investigated water circulation in a channel

[1]The publications of Jean Poiseuille, Henry Darcy, Fanning, von Mises, and Johann Nikuradse on the subject appeared in the year 1841, 1857, 1877, 1914, and 1933, respectively [www.wikipedia.org].

Downloaded By: [Technische Universiteit - Eindhoven] At: 14:34 14 June 2009

Downloaded By: [Technische Universiteit - Eindhoven] At: 14:34 14 June 2009

having $D_{hyd} \approx 200$–1923 μm and obtained good agreement with conventional channel theory.

Agostini et al. [12] have done friction factor and heat transfer coefficient experiments with liquid flow of R134a in rectangular mini-channels. Two test sections made of aluminum multiport extruded tubes (Tube 1: 1.11 mm and Tube 2: 0.72 mm) were tested. Literature correlations available for large tubes were found to predict their results reasonably well. Laminar to turbulent transition occurred around Re ≈ 2000. Also, Agostini et al. pointed out the importance of estimating uncertainties in reporting data on mini-channels.

Morini [13] has summarized the experimental work in mini-/micro-channels done until 2004. It is pointed out that in many cases the experimental data of Poiseuille number (Po) and Nusselt number (Nu) disagree with the conventional theory, but they also appear to be inconsistent with each other. Several reasons have been proposed to account for these differences. Rarefaction/compressibility effects, viscous dissipation, electro-osmotic effects, property variation effects, channel surface conditions (relative roughness and morphology), and experimental uncertainties have been invoked to explain the anomalous behavior of transport mechanisms through micro-channels.

Steinke and Kandlikar [14, 15] point out the importance of specifying exact boundary conditions for comparison of data from various sources. For example, in many studies, the heat flux is only applied to three sides of the channel, while, for comparative analysis, a uniformly applied heat flux is invoked. Also, since the heat transfer in mini-/micro-channels is very large, the associated differential temperatures are small. They highlight the importance of accurate temperature measurements for estimating transfer coefficients. They also point out, as many others have done in the past, that simultaneously developing flows are the most complex, and much more accurate data are needed in this regime.

Hetsroni et al. [16, 17] have analyzed and reviewed a large body of data in circular, triangular, rectangular, and trapezoidal mini-/micro-channels with D_{hyd} from 60 μm to 2000 μm. They discuss the effects of geometry, axial heat flux due to thermal conduction through the working fluid and channel walls, and energy dissipation in the fluid. They also discuss the entrance effects (inlet and outlet manifold design), effect of wall roughness, interfacial effects, and measurement accuracy. As regards surface roughness, they also conclude, as did Schlichting [18] in the classical text, that the presence of roughness on the wetted pipe surface favors an early laminar to turbulent flow transition. A need for a systematic approach to quantify the effect of surface roughness is also highlighted.

Reynaud et al. [19] have also undertaken pressure drop and heat transfer measurements of mini-channels ranging from 300 μm to 1.12 mm. All their experimental results are largely in good agreement with classical theory of conventional channels. Some observed deviations are explained either by macroscopic effects (mainly entry and viscous dissipation) or by imperfections of the experimental apparatus.

Kandlikar et al. [20] and later Taylor et al. [21] point out that since the modern mini/micro fluidic systems routinely violate the 5% relative roughness threshold, as set forth by the classical works of Nikuradse, Moody, etc. mentioned earlier, due to the inherent limitations of microfabrication techniques, there is a need to modify the Moody diagram. They propose a concept of $D_{cf}(D_{cf} = D_t - 2e)$. They redefine Re and f_{darcy} based on the constricted flow diameter just described; the Moody diagram was also re-plotted with these new definitions. Later, they tested various mini-/micro-channels and found that the transition from laminar to turbulent flow is seen to occur at Re well below 2100 because of roughness effects.

Recently, Caney et al. [22] tested a 1.0 mm^2 aluminum rectangular channel 420 mm long with flow Re ≈ 310–7790. They found that the experimental Poiseuille number and Nusselt number show a good agreement with classical correlations for conventional channels when appropriate corrections are invoked.

Thus, it can be concluded from the literature that most of the discrepancies in the reported data, especially on the mini-channel regime ($3\text{ mm} \geq D_{hyd} \geq 200$ μm), can be largely attributed to experimental uncertainties, sensor intrusion, effect of roughness, inlet/outlet manifold design, and proper control of exact boundary conditions in the experiment. Also, data on simultaneously/singly developing flows is not abundant. The present study is an attempt in this direction.

EXPERIMENTAL DETAILS AND DATA REDUCTION

The main parameters of interest for the present study are the differential pressure drop across the array and the spatial temperature distribution on the channel array walls and the working fluid, leading to spatial Nu_x data being desired under different flow conditions.

Hardware Description

A schematic of the setup is shown in Figure 1, while Figure 2, a–d, shows the details of the mini-channel test section. It

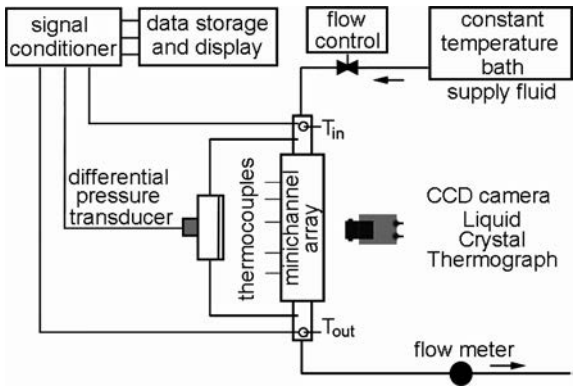

Figure 1 Schematic layout of the experimental setup.

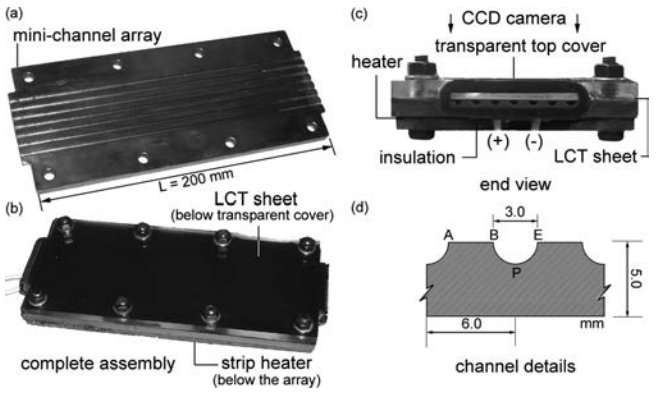

Figure 2 Details of the mini-channel array: (a) copper plate with mini-channels, (b) complete assembly of the array, (c) end view of the array, and (d) single channel details.

consists of an array of seven parallel semicircular mini-channels ($D = 3.0$ mm, $D_{hyd} = 1.83$ mm, $L = 200$ mm, pitch 6.0 mm) machined on a copper plate ($200 \times 85 \times 5$ mm^3). Channel roughness parameters are measured by a laser profilometer (Mahr; vertical resolution 1 nm, horizontal resolution 0.1 μm) and found to be $Ra = 3.17$ μm with $D_h/e = 577$. The working fluid at a fixed temperature, coming from the constant-temperature circulator bath, is allowed to pass through the mini-channel array via large inlet/outlet headers/plenums to maintain minimum inlet turbulence level. The inlet plenum has a gradually converging section followed by a straight rectangular section. The outlet plenum has a straight rectangular section followed by a gradually diverging section. The pressure transducer tappings are 50 mm away from the inlet and exit of the test section array, respectively. The area of cross section of the plenum is about 25 times that of the total projected flow area of the mini-channel array. Owing to the fact that the mini-channel array is considerably long, the friction/acceleration components of the pressure drop in the inlet/outlet plenums were estimated to be negligible as compared to the pressure drop in the mini-channel array. A piezoelectric strain gauge pressure transducer (Honeywell, accuracy 0.1%FS, NIST traceable calibration) measures the differential pressure across the channel geometry. Flow rates from $200 < Re < 4000$ are possible with the flow rate controller. A surface-mountable mica strip heater ($200 \times 90 \times 1$ mm^3), controlled by a digital power variac (accuracy ±0.1 V, 0.01 A), is attached below the copper plate to heat the incoming working fluid. Data acquisition is done with a high-speed 16-bit PCI-4351 card (National Instruments). The actual experimental flow velocities are in the range of 0.1 m/s to 1.0 m/s and the applied heat fluxes are in the range of 0.6 W/cm^2 to 2.0 W/cm^2 based on semicircular channel base area ($0.5\pi \cdot D \cdot L$).

Temperature Measurements by TLC

Conventional thermometry (e.g., with thermocouples) can only measure temperatures at discrete locations; detailed spatial flow field information cannot be generally obtained. Moreover, for measurements on mini/micro scales, spatial constraints and sensor intrusion in the flow restricts the information accuracy. In this background, liquid crystal thermography (LCT) technique has been employed in this study. An encapsulated 125-μm-thick thermochromic liquid crystal (TLC) sheet and a transparent 12.0 mm thick polycarbonate insulation backing plate cover the top surface of a mini-channel array, as shown in Figure 2. TLCs react to changes in temperature by changing color. Liquid crystals have chiral (twisted) molecular structures and are optically active mixtures of organic chemicals turning from colorless (black against a black background) to red at a given temperature and, as the temperature is increased, pass through the other colors of the visible spectrum in sequence (orange, yellow, green, blue, violet) before turning colorless (or black) again at a higher temperature. The color changes are reversible; on cooling, this color change sequence is reversed. Thus, the local spatial temperature distribution can be captured by a digitizer (e.g., a CCD camera) and suitably quantified in 8/16-bit pixel-specific information. This pixelized response, corresponding to the local temperature, will be usually available in the form of relative intensities in three primary colors, viz. red, green, and blue (RGB). To compare these with the temperature, the digitizer response need to be reduced to a single value. This is done by converting the pixel RGB values to HSI (hue, saturation, and intensity) color system and choosing the hue parameter to scale with temperature (refer to Appendix for details of this conversion scheme). The important reason to choose "hue" as the discriminating parameter is the fact that hue value calculated for one color remains constant for large changes in image intensity or illumination. Thus, to a large extent the measurement becomes independent of the illumination [23]. Calibration is the most critical element of success with LCT technique; in situ calibration was carefully conducted under controlled conditions using a high-accuracy kelvimat (HAAKE DC10K20). It is important to perform the calibration "in situ" so that identical conditions exist during calibration and subsequent experiments. Therefore, calibration was done on the same mini-channel array prior to experiments. In fact, if the experiments last for longer duration, in situ calibration is recommended after every couple of days. Without the heater power, water was circulated in the array at a fixed temperature by the kelvimat. In addition to the inlet and outlet thermocouples, two more thermocouples were embedded in the wall of the array and placed along the axial direction for additional assurance and datum reference. In this manner, after steady state is reached, the complete array was isothermal and the LCT sheet placed on the top depicted a single unique hue value. Figure 3 shows the typical calibration curve between obtained hue value and the operating isothermal plate temperature. The streamwise spatial variation of wall and the fluid temperatures respectively in each channel, depicted by the TLC sheet, are captured via a color CCD camera (Basler-A202KC). We estimate the overall accuracy of the process to be within ±0.46°C. This includes uncertainty in the primary thermocouple sensors, sensitivity of hue calibration, and standard error estimate for curve fitting [23].

Downloaded By: [Technische Universiteit - Eindhoven] At: 14:34 14 June 2009

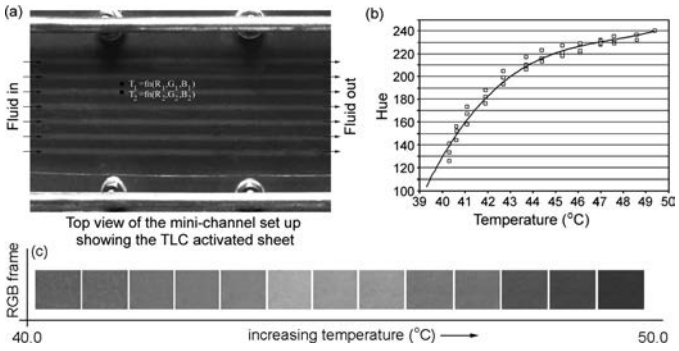

Figure 3 (a) Typical LCT image of the array; (b) calibration curve between hue and temperature; and (c) actual RGB images captured during calibration.

Nusselt Number Estimation

Next we discuss the way $Nu_{x,exp}$ at any axial location x along the channel has been estimated from the raw data. Referring to Figures 2 and 4 (the latter figure shows the computational domain, which is explained in the next section), the TLC sheet gives the spatial surface temperature of surface area A-B-C-D located on the channel wall and area B-E-F-C where the fluid is flowing (top view T captured by the CCD camera). For calculating $Nu_{x,exp}$ we estimate the average temperatures of control surface S1 (T_{wall}) and S2 (T_{fluid}). These control surfaces are chosen to be typically about 10 mm^2. The heat flux required to calculate $Nu_{x,exp}$ is obtained by dividing the net electrical power input at the base plate minus the heat losses, by the semicircular channel wall area ($0.5\pi \cdot D \cdot L$), and assuming this flux to be a constant in the streamwise direction. The heat losses to the environment are estimated to be 7.6–12% depending on the experimental conditions. The uncertainty in $Nu_{x,exp}$ is estimated to be on the order of 27%. $Nu_{x,exp}$ thus obtained does not correspond to the classical definition of wall Nu_x for internal flows. Nevertheless, such a compromise has been adopted because we require continuous streamwise temperature for analyzing simultaneously developing flows. We further argue that the $Nu_{x,exp}$ values thus obtained are expected to be much superior to those estimated from isolated data points obtained from thermocouples located along the channel. Frequently, average T_{fluid}at any section is also estimated from a linear interpolation of T_{in} and T_{out}, which leads to errors in estimating Nu_x. Thermocouples too either interfere with the flow and/or wall correction has to be employed because of proximity issues [22]. These limitations of conventional thermometry are more pronounced in mini/micro physical domains. The present experimental TLC arrangement allows for continuous measurement of wall and fluid temperatures at high spatial resolution, albeit with some limitations for estimating true wall Nu_x as just explained. To overcome these shortcomings, the complimentary computations not only provide data for exact comparison with $Nu_{x,exp}$ as done here, but they also provide information on the true wall Nu_x. Moreover, computations can also highlight the effect of Biot number ($Bi = h \cdot D_{hyd}/k_s$) of the channel material on Nu_x and thereby we can estimate the effect of axial conduction in the channel wall or substrate.

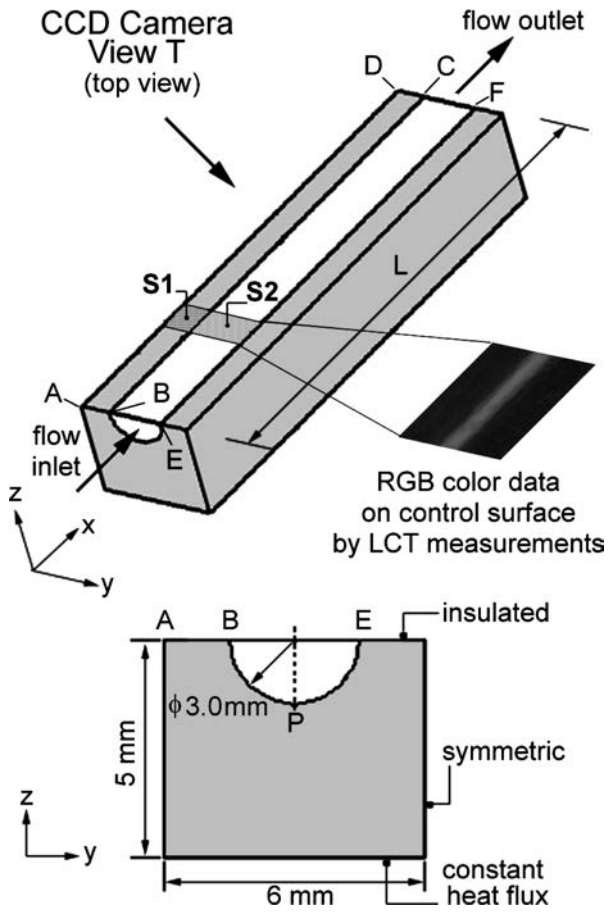

Figure 4 Computational domain for single channel with applicable boundary conditions; inset shows the corresponding LCT image as seen from the top for the purpose of analyses.

COMPUTATIONAL MODELING AND SIMULATIONS

In the case of fully developed flows or isolated hydrodynamic or thermal entry problems, since the energy equation is linear and homogeneous (neglecting source terms, viscous dissipation, and flow work terms), linear superposition techniques are relatively easy to apply for obtaining analytical solutions. In contrast, for simultaneously developing flows, even for singly connected ducts, linear superposition is quite impractical [1, 2]. For multiply connected ducts, as in the present case, this is a formidable task, almost quite impossible; only a very few analytical solutions exist for simple geometries like circular channels and parallel plates. In this background, for the present problem, a 3D computational domain, as shown in Figure 4, consisting of hexahedral grids (total 0.6 million grid points) was constructed using ICEM-CFD and solved on a Fluent platform for steady-state conjugate heat transfer conditions. Grid independence test was separately conducted to ascertain the validity and quality of

Downloaded By: [Technische Universiteit - Eindhoven] At: 14:34 14 June 2009

the generated grid. The numerical domain was formulated with exactly the same boundary conditions as encountered in the experimental setup. For a given fixed inlet mass flow rate of the working fluid, the flow was allowed to hydrodynamically and thermally develop in the channel. Since the applicable Prandtl number (Pr) was between 4 and 4.5, circumstances represent a combined entry length problem. Simulations were carried out by incorporating standard laminar flow approximations or a realizable k–ε model, as found appropriate vis-à-vis the experimental results.

RESULTS AND DISCUSSION

The thermal/fluid flow parameters and test section geometry were chosen in such a manner that the flow was always partly developing, both hydrodynamically and thermally, in the channels. Figure 5a and b, shows the hydrodynamic and thermal entry length estimations with respect to the flow Reynolds number; standard equations are used for these estimations, as shown [4]. In this figure, laminar to turbulent transition is depicted at Re = 1500, which roughly corresponds to the present experiments (experimental results will be presented later). As can be seen from Figure 5a, for the present case of 200 mm channels, to a large extent, hydrodynamically developing flow exists in the channel throughout the laminar regime. Under turbulent conditions, flow develops rather quickly if we consider that the estimate of $L_{e,hyd} = 10D_h$ is applicable. If the upper limit of $L_{e,hyd} = 60D_h$ is considered valid, then in this case, too, flow is hydrodynamically developing in nature, to a large extent of the channel. It should be noted, however, that Figure 5 can, at best, be treated as a theoretical guideline; in practical reality the boundaries between "developing" and "fully developed" may be fuzzy due to intrinsic perturbations and inherent system/hardware design limitations, which induces "non-ideal" flow characteristics.

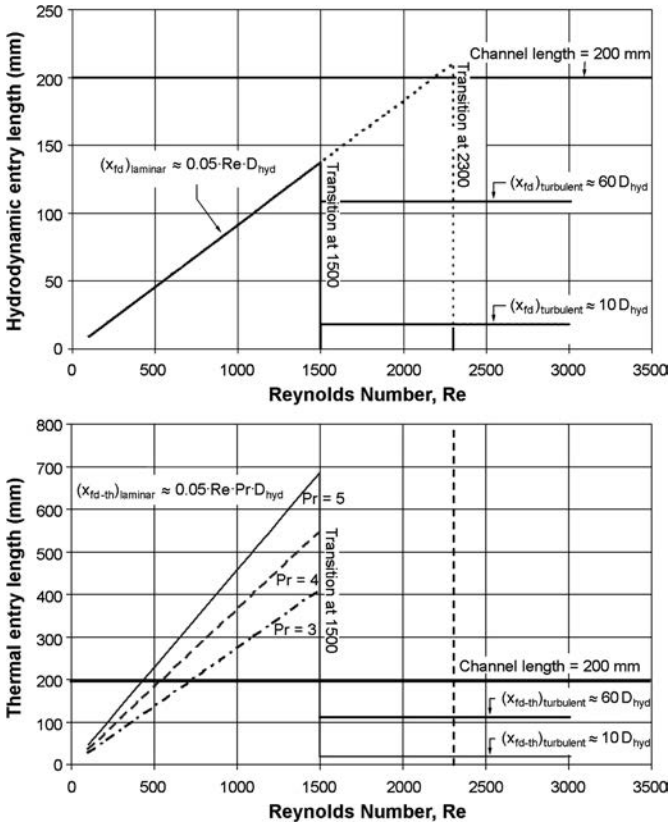

Figure 5 Variation of (a) hydrodynamic entry length and (b) thermal entry length with flow Re.

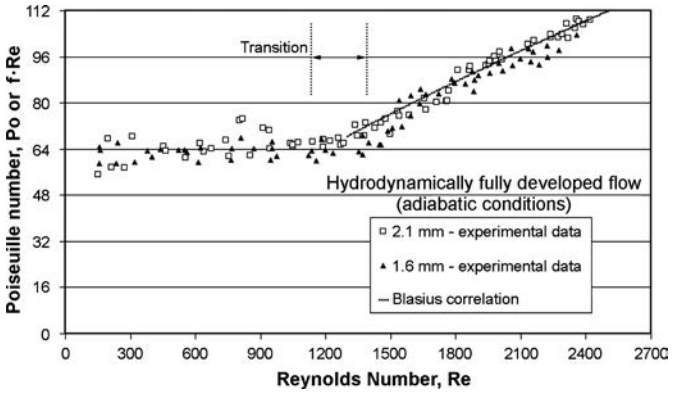

Figure 6 Po vs. Re for benchmark experiments done on hydrodynamically fully developed flow under adiabatic conditions.

As regards to the thermal boundary layer development (refer to Figure 5b), since the applicable Pr is in the range of ≈ 4–4.5, under laminar flow conditions, flow is thermally developing over the entire channel length (unless for flow Re below about 500, in which case the flow will be thermally partly "developing + developed" in the channel). Given the fact that typically a length of $\geq 10D_{hyd}$ is considered sufficient for full hydrodynamic turbulent flow development, there is a possibility that turbulent flow fully develops within the channel length, as suggested by Figure 5a and b.

Before commencement of experiments on a semicircular channel array, baseline experiments were performed on fully developed flow in circular channels (D: 2.1 mm and 1.6 mm) to benchmark the differential pressure measurements. The consolidated results for the variation of Po with flow Re is shown in Figure 6. As can be clearly seen, both the laminar and turbulent flows match the classical results quite accurately (Po ≈ 64 for laminar flow and following Blasius correlation for turbulent regime [3]) except for the fact that there is an early transition to turbulence, in the range ∼1200–1400. This observation is also similar to the recent trends in the literature, as discussed earlier, wherein flow transitions have occurred earlier than the conventional Re range.[2]

Having benchmarked the differential pressure measurement for fully developed internal flows, tests were performed on the semicircular array. Thermo-hydrodynamic measurements were

[2]It should, however, be noted here that some other contemporary studies do also report that transition in mini-/micro-channels follows conventional transition trends (for example refer to [24, 25]).

Downloaded By: [Technische Universiteit - Eindhoven] At: 14:34 14 June 2009

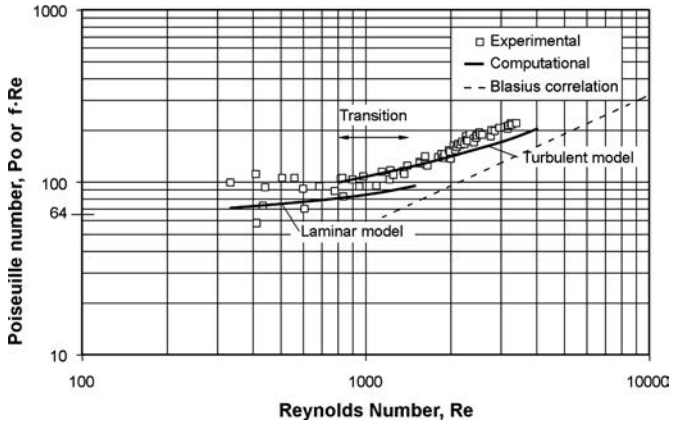

Figure 7 Po vs. Re for the semicircular array.

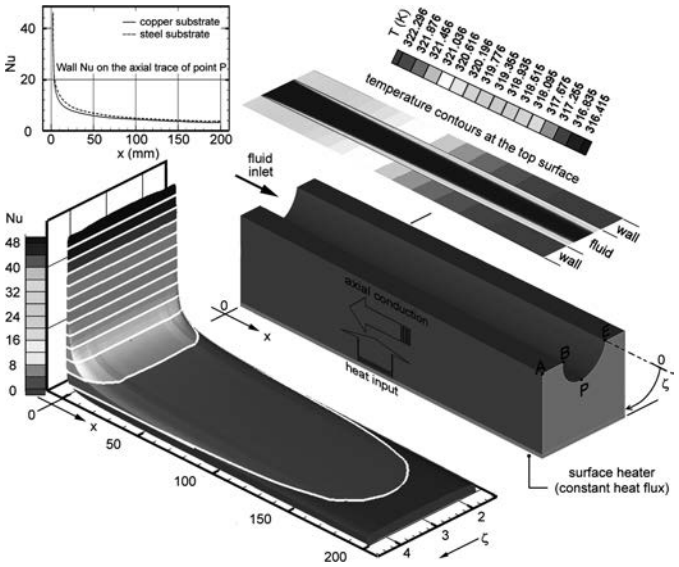

Figure 8 Three-dimensional variation of Nu in the semicircular channel at flow Re = 1080. Also shown is the temperature variation on the top surface of the channel. Inset shows the variation of the wall Nu on the longitudinal trace of point P for two situations: (i) copper substrate, low Bi situation, and (ii) steel substrate, high Bi situation.

simultaneously done; the conditions were always "simultaneously developing," as per Figure 5. Figure 7 presents the variation of Po with Re for the semicircular array. The numerical predictions are also shown on it, along with the Blasius correlation [3], representing the fully developed turbulent flow case. As can be seen, for simultaneously developing laminar flows, the Po is considerably higher than a value of 64 (circular section) and 63.1 (semicircular section), which is applicable for fully developed laminar conditions. This increase is due to the additional momentum flux transfer apart from the frictional component that is encountered in developing flows. In other words, the net pressure gradient constitutes contributions from (i) fully developed profile and (ii) accumulated incremental wall shear due to additional momentum flux transfer during hydrodynamic flow development. As can be seen, flow transition occurs at about Re ∼900–1500; thereafter, Po varies strongly with the flow Re. Numerical predictions are closely matching the experiments. In the turbulent region, due to the inherent limitations of the k–ε model to handle near-wall turbulence, a realizable k–ε model has been employed that provides better estimates. The latter model shows superior performance over the standard k–ε model as, consistent with the physics of turbulent flows and mathematical constraints on the Reynolds stresses, it prevents the turbulence kinetic energy from becoming negative [26].

Figure 8 shows a typical computational result for the three-dimensional variation of Nu on the entire semicircular channel wall at flow Re = 1080 (laminar flow consideration). In the figure, ζ represents the curvilinear coordinate along the circumference of the semicircular wall. The channel inlet experiences the highest Nu; the flow is still simultaneously developing at the exit. At any cross section, Nu_x is highest on the axial trace of point P (refer to Figure 8) and lowest at the points B and E, as shown. The inset shows the wall Nu on the axial trace of point P for two distinct situations. As can be clearly seen, the Nu for a copper substrate (k = 380 W/mK) is lower than that for a steel substrate (k = 14 W/mK), with this difference being most pronounced near the entry region where the maximum amount of heat is being transferred to the fluid. The fact that there is a considerable wall conduction effect is clearly highlighted; the constant heat flux boundary condition applied at a distance away from the channel wall tends to be manifested as a "pseudo-constant-temperature" boundary condition to the incoming fluid, thereby lowering the effective wall Nu. This happens due to the temperature equalization happening because of the conducting walls of the substrate/channel material, as shown in Figure 8. Thus, for low Bi number situations, interpretation of experimental data on Nu needs careful scrutiny since one-dimensional heat conduction approximation in the substrate/wall, which is frequently incorporated, is not valid. The issue of true boundary condition experienced by the fluid and its experimental control/quantification is even more important in microscale geometries and has been highlighted in the recent literature (e.g., refer to [27]–[29]).

Figure 9, a–e, shows the main experimental and computational results for Nu_x obtained in this study, plotted against nondimensional distance x^* along the channel. The uncertainty bars have been estimated by a standard single-sample analysis procedure outlined elsewhere [23, 30, 31]. In these figures, computational Scheme 1 represents the results calculated exactly as per the process employed for obtaining the $Nu_{x,exp}$ (i.e., taking control surfaces S1 and S2, as referred to earlier, on the experimental TLC data and corresponding locations on the computational domain). Computational Scheme 2 represents the variation of true wall Nu_x at the streamwise trace of point P (refer to Figures 4 and 8), located on the midpoint of the semicircular arc of the channel wall. Incidentally, as has been noted earlier, at any cross section along the channel, this midpoint of the semicircular arc has the highest local Nu. Thus, results for Nu with computational Scheme 2, at any specified axial location along the channel, represent the upper bound of wall Nu_x, at that

Downloaded By: [Technische Universiteit - Eindhoven] At: 14:34 14 June 2009

Downloaded By: [Technische Universiteit - Eindhoven] At: 14:34 14 June 2009

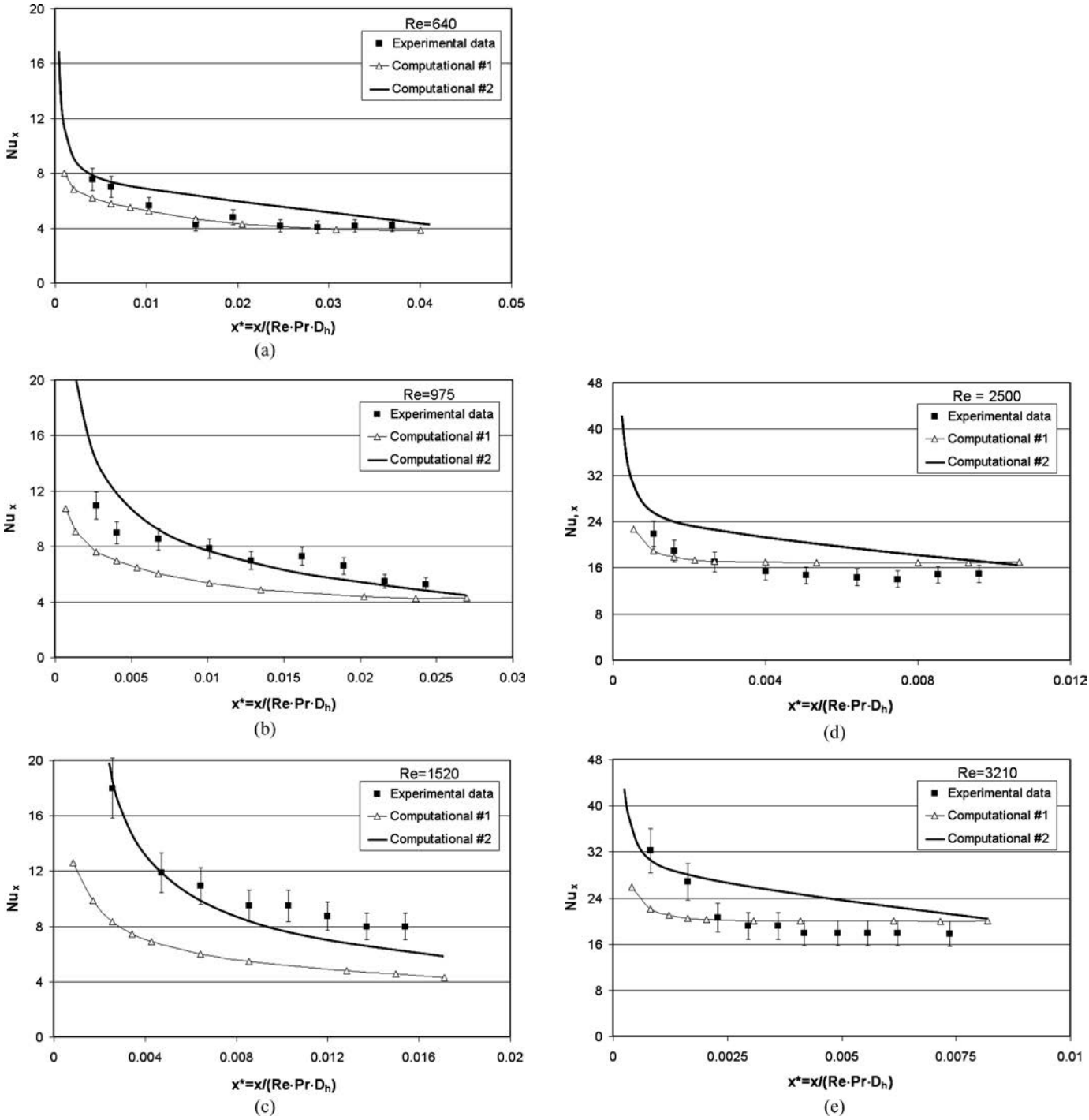

Figure 9 Axial variation of Nu_x along the channel length: (a) Re = 640, (b) Re = 940, (c) Re = 1520, (d) Re = 2500, and (e) Re = 3210.

location. For Figure 9, a–c, computations have been performed by considering a laminar flow model. At low Re (= 640, Figure 9a), the computational results closely match the experiments; in this case the flow also develops rather quickly (as indicated in Figure 5).

As the Re increases, flow transitions commence and a laminar flow approximation, as done in obtaining the computational results of Figure 9b and c, starts showing its limitations. The $Nu_{x,exp}$ progressively becomes higher than the predictions because of the enhanced transport interactions due to commencement of flow transition. Beyond Re = 1500 the use of laminar flow-based computations was found to be quite unacceptable and therefore a realizable k–ε model was employed to generate computational results depicted in Figure 9d and e. As can be seen, this considerably improves the comparison with the $Nu_{x,exp}$.

Downloaded By: [Technische Universiteit - Eindhoven] At: 14:34 14 June 2009

SUMMARY AND CONCLUSIONS

Developing flows are characterized by large species transport coefficients. This article presents the application of liquid crystal thermographic technique for determining the spatial temperature distribution in developing internal flows in a mini-channel array. Simultaneously developing flow through a mini-channel array consisting of seven semicircular channels of diameter 3.0 mm (D_{hyd} = 1.83 mm, L = 200 mm) has been considered under conjugate thermal conditions. Flow Re was varied from 300 to 3200, while flow Pr was maintained in the range of 4–4.5. For comparison of the data, a complete 3D computational solution was also attempted; the computational domain and boundary conditions were exactly matching those applied during the experiments. The main conclusions of the study are:

(i) Developing flows provide very high transfer coefficients in the entrance regions and therefore of interest for mini-/micro-scale high flux transfer applications.
(ii) In general, the conventional theory that predicts thermo-hydrodynamics of internal flows is well applicable for the mini-channels used in this study (D_{hyd} ~1.83 mm). No additional physical effects were observed.
(iii) Experimental data suggests an early laminar to turbulent transition in the range of Re ≈ 800–1500. This is primarily attributed to the channel roughness morphology.
(iv) The experimental Poiseuille number under laminar and turbulent conditions closely matched with those generated by the 3D computational model. For turbulent flow modeling, a realizable k–ε model gave much better results than a standard k–ε model.
(v) The effect of wall conduction in the substrate on the Nusselt number variation was clearly observable. For low Bi situations typically encountered with high thermal conductivity substrates, these shifts in boundary condition, as experienced at the wall, must be accounted for, especially in the entrance regions of the flow. The approximation of one-dimensional diffusional heat transport in the pipe/substrate wall is not always appropriate.
(vi) Although liquid crystal thermography has some limitations, primarily traceable to calibration issues and temperature range of applicability, it is nevertheless a very attractive experimental technique, especially in the mini–micro regime of heat transfer experiments, wherein conventional thermometry may be quite unsuitable.

ACKNOWLEDGMENTS

The work is partially funded by an IITK Faculty Initiation Grant (number IITK/ME/20050019) and the Department of Science and Technology, Government of India DST (IITKDST/20060304). The contributions of Mr. Avinash Chopde, NIT, Nagpur, India, for additional measurements (under the IIT Kanpur-SURGE program) and discussions with Dr. Arun Saha are also acknowledged.

NOMENCLATURE

Bi	Biot number ($h \cdot D_{hyd}/k_s$)
D	diameter (m)
e	roughness height, rms value (m)
f or f_{darcy}	coefficient of friction
h	heat transfer coefficient (W/m^2K)
k	thermal conductivity (W/mK)
L	length (m)
Nu	Nusselt number ($h \cdot D_{hyd}/k_{liq}$)
Po	Poiseuille number ($f \cdot Re$)
Pr	Prandtl number (ν/α)
Ra	average surface roughness (m)
Re	Reynolds number ($\rho U L/\mu$)
T	temperature (°C or K)
U	average velocity (m/s)
x	streamwise distance (m)
x*	nondimensional distance ($x/Re \cdot Pr \cdot D_h$)

Greek Symbols

α	thermal diffusivity (m^2/s)
μ	dynamic viscosity (N-s $/m^2$)
ρ	mass density (kg/m^3)
ν	kinematic viscosity (m^2/s)
ζ	curvilinear coordinate

Subscripts

cf	confined or constricted flow
e	entry
exp	experimental
fd	fully developed
hyd or h	hydraulic
in	inlet
liq	liquid
out	outlet
s	solid
th	thermal
t	tube

Acronyms

TLC	thermochromic liquid crystal
LCT	liquid crystal thermography

Downloaded By: [Technische Universiteit - Eindhoven] At: 14:34 14 June 2009

REFERENCES

[1] Shah, R. K., and London, A. L., *Laminar Flow Forced Convection in Ducts*, Academic Press, New York, 1978.

[2] Kays, W. M., and Crawford, M. E., *Convective Heat and Mass Transfer*, 3rd ed., McGraw-Hill, New York, 1993.

[3] Bejan, A., and Kraus, A. D., *Heat Transfer Handbook*, John Wiley & Sons, New York, 2003.

[4] Kandlikar, S. G., Garimella, S., Li, D., Colin, S., and King, M., *Heat Transfer and Fluid Flow in Minichannels and Microchannels*, Elsevier, New York, 2006.

[5] Kandlikar, S. G., and Grande, W. J., Evolution of microchannel flow passages—Thermohydraulic performance and fabrication technology, *Heat Transfer Engineering*, vol. 24, no. 1, pp. 3–17, 2003.

[6] Wu, P. Y., and Little, W. A., Measurement of friction factor for the flow of gases in very fine channels used for micro miniature Joule-Thompson refrigerators, *Cryogenics*, vol. 23, no. 5, pp. 273–277, 1983.

[7] Tuckerman, D. B., and Pease, R. F., High performance heat sinking for VLSI, *IEEE Electronic Device Letters*, vol. EDL-2, pp. 126–129, 1981.

[8] Wang, B. X., and Peng, X. F., Experimental investigation on liquid forced convection heat transfer through micro-channel, *International Journal of Heat and Mass Transfer*, vol. 37, Suppl. I, pp. 73–82, 1994.

[9] Peng, X. F., and Peterson, G. P., Convective heat transfer and flow friction for water flow in micro-channel structures, *International Journal of Heat and Mass Transfer*, vol. 39, no. 12, pp. 2599–2608, 1996.

[10] Adams, T., Abdel-Khalik, S., Jeter, S., and Qureshi Z., An experimental investigation of single-phase forced convection in microchannels, *International Journal of Heat and Mass Transfer*, vol. 41, no. 6–7, pp 851–857, 1997.

[11] Gao, P., Le Person, S., and Favre-Marinet, M., Scale effects on hydrodynamics and heat transfer in two-dimensional mini and micro channels, *International Journal of Thermal Sciences*, vol. 41, pp. 1017–1027, 2002.

[12] Agostini, B., Watel, B., Bontemps, A., and Thonon B., Liquid flow friction factor and heat transfer coefficient in small channels: An experimental investigation, *Experimental Thermal and Fluid Science*, vol. 28, pp. 97–103, 2004.

[13] Luca Morini, G., Single-phase convective heat transfer in microchannels: A review of experimental results, *International Journal of Thermal Sciences*, vol. 43, pp. 631–651, 2004.

[14] Steinke, M., and Kandlikar, S. G., Single-phase liquid heat transfer in micro-channels, *Proceedings of ICMM2005—3rd International Conference on Micro-channels and Mini-channels*, Toronto, pp. 1–12, 2005.

[15] Steinke, M., and Kandlikar, S. G., Single-phase liquid friction factors in micro-channels, *Proceedings of ICMM2005—3rd International Conference on Micro-channels and Mini-channels*, Toronto, pp. 291–302, 2005.

[16] Hetsroni, G., Mosyak, A., Pogrebnyak, E., and Yarin, L. P., Fluid flow in micro channels, *International Journal of Heat and Mass Transfer*, vol. 48, pp. 1982–1998, 2005.

[17] Hetsroni, G., Mosyak, A., Pogrebnyak, E., and Yarin, L. P., Heat transfer in micro-channels: Comparison of experiments with theory and numerical results, *International Journal of Heat and Mass Transfer*, vol. 48, pp. 5580–5601, 2005.

[18] Schlichting, H., *Boundary Layer Theory*, 7th ed., McGraw-Hill, New York, 1979.

[19] Reynaud, S., Debray, F., Franc, J., and Maitre, T., Hydrodynamics and heat transfer in two-dimensional minichannels, *International Journal of Heat and Mass Transfer*, vol. 48, pp. 3197–3211, 2005.

[20] Kandlikar, S. G., Schmitt, D., Carrano, A. L., and Taylor, J. B., Characterization of surface roughness effects on pressure drop in single phase flow in minichannels, *Physics of Fluids*, vol. 17, no. 10, 2005.

[21] Taylor, J., Carrano, A., and Kandlikar, S. G., Characterization of the effect of surface roughness and texture on fluid flow—Past, present and future, *International Journal of Thermal Sciences*, vol. 45, pp. 962–968, 2006.

[22] Caney, N., Marty, P., and Bigot J., Friction losses and heat transfer of single-phase flow in a mini-channel, *Applied Thermal Engineering*, vol. 27, pp. 1715–1721, 2006.

[23] Muwanga, R., and Hassan, I., Local heat transfer measurements in microchannels using liquid crystal thermography: Methodology development and validation, *Journal of Heat Transfer*, vol. 128, pp. 617–627, 2006.

[24] Sharp, K. V., and Adrian, R. J., Transition from laminar to turbulent flow in liquid filled microtubes, *Experiments in Fluids*, vol. 36, pp. 741–747, 2004.

[25] Hwang, Y. W., and Kim, M. S., The pressure drop in microtubes and the correlation development, *International Journal of Heat and Mass Transfer*, vol. 49, pp. 1804–1812, 2006.

[26] Shih, T. H., Liou, W. W., Shabbir, A., Yang, Z., and Zhu J., A new k-e eddy-viscosity model for high Reynolds number turbulent flows—Model development and validation. *Computers and Fluids*, vol. 24, no. 3, pp. 227–238, 1995.

[27] Guo, Z. H., and Li, Z. X., Size effect on single-phase channel flow and heat transfer, *Int. Journal of Heat and Fluid Flow*, vol. 24, pp. 284–298, 2003.

[28] Herwig, H., and Hausner, O., Critical view on 'New results in micro-fluid mechanics': An example, *International Journal of Heat and Mass Transfer*, vol. 46, pp. 935–937, 2003.

[29] Kinglsey-Rowe, J. R., Lock, G. D., and Owen, J. M., Transient heat transfer measurements using thermochromic liquid crystal: Lateral-conduction error, *International Journal of Heat and Fluid Flow*, vol. 26, pp. 256–263, 2005.

[30] Kline, S. J., and McClintok, F. A., Describing uncertainties in single sample experiments, *Mechanical Engineering*, pp. 3–8, 1953.

[31] Moffat, R. J., Describing the uncertainties in experimental results, *Experimental Thermal and Fluid Science*, vol. 1, pp. 3–17, 1988.

Manoj Rao is presently working as a product design engineer in the Emerson Design and Engineering Center, Pune, India. Prior to this assignment he worked as a research associate at the Indian Institute of Technology Kanpur, India. He has obtained master's degree in thermal engineering from National Institute of Technology, Bhopal, India, in 2007. Currently he is working in the field of low- and high-flow designs of coriolis sensors.

Sameer Khandekar is an assistant professor of mechanical engineering at the Indian Institute of Technology Kanpur (IITK), India, where he has worked since September 2004. He obtained a master's degree in thermal engineering from IIT Kanpur (in 2000) and completed the doctoral assignment from University of Stuttgart, Germany (in 2004). He has also worked as a marine power plant engineer for four years. He has been awarded the George Grover Medal by the International Heat Pipe Committee for his work on pulsating heat pipes and a Young Scientist Award by the Department of Atomic Energy, India. He is presently working on experimental thermal-fluid engineering and two-phase heat transfer at mini/micro scales, pulsating heat pipes, and hydrogen generation.

Downloaded By: [Technische Universiteit - Eindhoven] At: 14:34 14 June 2009

APPENDIX

Converting RGB color space image to HSI space:
Step 1: Normalizing [R, G, B] values.

$$r = \left(\frac{R}{R+G+B}\right)$$

$$g = \left(\frac{G}{R+G+B}\right) \tag{A1}$$

$$b = \left(\frac{B}{R+G+B}\right)$$

Step 2: Getting normalized [H, S, I], i.e., [h, s, i] components.

$$h = \cos^{-1}\left\{\frac{0.5[(r-g)+(r-b)]}{[(r-g)^2+(r-b)(g-b)]^{\frac{1}{2}}}\right\}; h$$

$$\times \in [o, \pi] \text{for} b \le g \tag{A2a}$$

or

$$h = 2\pi - \cos^{-1}\left\{\frac{0.5[(r-g)+(r-b)]}{[(r-g)^2+(r-b)(g-b)]^{\frac{1}{2}}}\right\};$$

$$\times h \in [\pi, 2\pi] \text{for} b > g \tag{A2b}$$

$$s = 1.0 - 3 \cdot (\min|r, g, b|) \quad s \in [0, 1] \tag{A3}$$

$$i = \frac{1}{3}\left(\frac{R+G+B}{255}\right) \quad i \in [0, 1] \tag{A4}$$

Step 3: For convenience h, s, and i values are converted in the ranges of [0–360], [0–100], and [0–255], respectively.

$$H = \frac{h \times 180}{\pi}$$

$$S = s \times 100 \tag{A5}$$

$$I = i \times 255$$

As an example, we consider a particular pixel with:

$$[R, G, B] = [100, 150, 200]$$

Step 1: using Eq. (A1) we get [r, g, b] = [0.222, 0.333, 0.444].
Step 2: using Eq. (A2b) for b > g we get [h, s, i] = [1.167π, 0.333, 0.588].
Step 3: using Eq. (A5) we get [H, S, I] = [210, 33.3, 150].